ADVANCED FUNCTIONAL MATERIALS
www.afm-journal.de

Materials Views
www.MaterialsViews.com

In Situ Synthesis of Bipyramidal Sulfur with 3D Carbon Nanotube Framework for Lithium–Sulfur Batteries

*Lina Wang, Yu Zhao, Morgan L. Thomas, and Hye Ryung Byon**

A one-pot synthesis of three-dimensional carbon nanotube frameworks with bipyramidal sulfur particles and the application of these materials for a cathode in lithium–sulfur (Li–S) battery are reported. By simple mixing of multi-walled carbon nanotubes (MWCNTs), sulfur powder, and capping agents in water/tetrahydrofuran, micrometer bipyramidal sulfur particles enclosed with MWCNTs are synthesized. The MWCNTs spontaneously form a 3D conducting network inside and outside the sulfur particle. Along the edge of MWCNT framework, a sulfur particle-free region is present, which comprises ≈35 vol% based on the total volume. These sulfur-MWCNT bipyramidal particles are mixed with conductive carbon additive to prepare binder-free cathode for Li–S cells. The Li–S cells deliver a specific discharge capacity of ≈1600 mAh g^{-1} at 0.05 C on the first cycle. In particular, these Li–S cells show high rate stability and Coulombic efficiency with deep discharge and charge (1.0–3.0 V vs Li/Li^+). This resultant performance can arise from 1) homogeneous distribution of the conducting MWCNT framework and the carbon additive coating layer on the sulfur particle, which allow rapid Li^+ ion/electrolyte diffusion and mitigation of polysulfide shuttle, respectively, and 2) the sulfur-free buffer space accommodating volume expansion. It is expected that this new cathode design with the simple synthetic process can reduce the number of preparation steps, thus allowing the construction of a low-cost Li–S battery.

1. Introduction

Rechargeable lithium–sulfur (Li–S) batteries have been extensively investigated in recent years owing to theoretically high specific capacity (1675 mAh g^{-1}), low cost, and environmentally benign sulfur.[1,2] Laboratory scale Li–S cells have demonstrated a reliable high capacity (>1000 mAh g^{-1} at a current rate of less than 1 C (1 C = 1675 mA g^{-1})) based on a Li–S electrochemical reaction ($16Li + S_8 + 16e^- \rightarrow 8Li_2S$) for the first discharge, which holds promise for the creation of a new generation of energy storage with high energy density. To employ these Li–S cells practically, however, further development is needed to retain the high capacity during cycling. The poor cyclic performance mostly arises from active material loss and degradation of cathode structure by a polysulfide shuttle in nonaqueous electrolytes.[1–3] The highly soluble lithium polysulfides (Li_2S_x, $4 \le x \le 8$) as intermediates can diffuse between the lithium anode and cathode, and are precipitated on the electrodes. When the polysulfide species are deposited on the cathode as insoluble discharge products (Li_2S_2 and Li_2S) by the reduction, the cathode suffers from a 70–80% volume expansion. In addition, these insulating discharge products increase the internal resistance, which causes an irreversible reaction during cycling.

To mitigate these challenges, diverse designs of cathode have been intensively studied in the Li–S cells. The core idea was to confine the sulfur within a conducting carbon matrix and allow an adequate buffer space for the volume expansion during discharge. Representatively, micro/mesoporous structures obtained by CMK-3,[3] ordered mesoporous carbon,[4] metal-organic frameworks[5] or anodic aluminum oxide (AAO)[6] have been employed to template cathode structures for encapsulation of nanometer-sized sulfurs. Carbon nanotubes/fibers,[1,7] polymer/conducting polymers[8,9] and graphene/graphene oxide sheets[10–12] have been also used to enclose the sulfur particles. These structures have alleviated the parasitic shuttle effect and maintained the electronic conductivity in the cathode, which have contributed to the enhanced capacity retention and reversible reaction. However, these cathodes were prepared by cumbersome synthetic processes. To make the sulfur-encapsulated micro/mesoporous structure via the templates, multiple synthetic steps were demanded, for example, construction of the hard template, then carbon coating and finally sulfur impregnation.[3–6] The cathode structures comprised of carbon nanotubes, polymers or graphene sheets were prepared by relatively simplified processes. However, these structures provided limited buffer space with a random arrangement, which may cause mechanical stress during volume expansion.[1,8,10,11,13]

Here, we present a new cathode structure consisting of bipyramidal sulfur particles and 3D multi-walled carbon nanotube (MWCNT) frameworks for the Li–S cells using a simple process. The sulfur particle and MWCNT frameworks are in situ synthesized without the use of a template. The 3D MWCNT framework provides high electrical conductivity owing to the uniform distribution of conducting tubes inside of the sulfur particle and affords ≈35 vol% sulfur-free buffer space. In addition, a layer of conductive additives (Ketjenblack (KB) carbon)

Dr. L. Wang, Dr. Y. Zhao, Dr. M. L. Thomas,
Dr. H. R. Byon
Byon Initiative Research Unit (IRU)
RIKEN, 2–1 Hirosawa, Wako, Saitama, 351–0198, Japan
E-mail: hrbyon@riken.jp

DOI: 10.1002/adfm.201302915

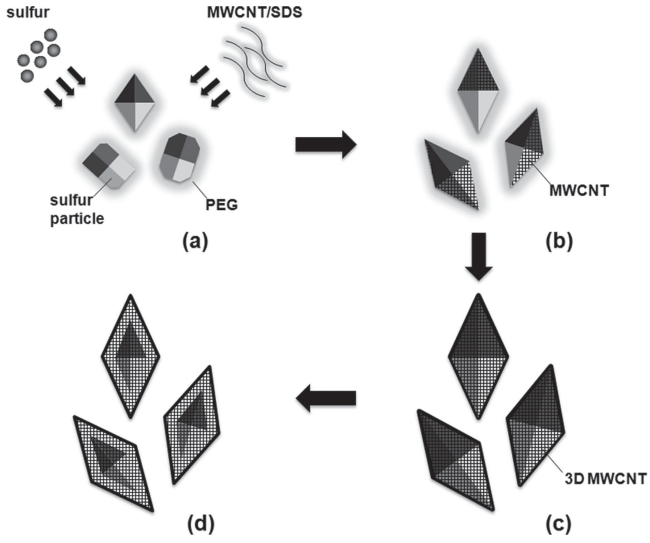

Figure 1. Schematic illustration of synthesis process of S-MWCNT. a) The sulfur particle rapidly nucleates and grows at initial stage. b) During the intermediate growth stage, MWCNT coats the sulfur particle and the irregular shaped sulfur gradually adjusts its shape and size and becomes larger. c) At termination stage, bipyramidal shaped sulfur particles with MWCNT frameworks (S-MWCNT) can be formed. d) By sulfur densification, the S-MWCNT allows a sulfur-free region.

shielding the S-MWCNT can impede the polysulfide shuttle and increase electrical conductivity further. Li–S cells employing the S-MWCNT display high rate stability and ≈100% Coulombic efficiency even with deep discharge/charge.

2. Results and Discussion

2.1. In Situ Synthesis of Bipyramidal Sulfur with 3D Carbon Nanotube Framework (S-MWCNT)

The S-MWCNT structures were prepared by a one-pot synthesis. Briefly, acid-treated MWCNTs, which were dispersed in the aqueous solution with excess sodium dodecyl sulfonate (SDS) and polyethylene glycol (PEG), were mixed with sulfur-saturated tetrahydrofuran (THF) under vigorous stirring. After 12 h aging at room temperature, the S-MWCNT product was washed, cooled (0 °C), and dried in a vacuum oven at 50 °C (see Experimental Section). **Figure 1** depicts the process of in situ S-MWCNT formation. The sulfur particles are nucleated and grown immediately when the sulfur-saturated THF is added to the aqueous solution containing the MWCNT/SDS stabilizer. We could observe rapidly changed liquid mixture color (bluish) and large sulfur particles with various shapes during initial 10 min (Figure 1a and Supporting Information, Figure S1a). The MWCNTs wrapped by the SDS then start to enclose the sulfur surfaces (Figure S1b, Supporting Information). At the same time, the sulfur particles gradually grow and adjust their shape and size with the aid of the PEG acting as a capping agent (Figure S2, Supporting Information),[10] which results in incorporation of MWCNTs into the sulfur particles (Figure 1b). The growth of sulfur particles can be terminated as a bipyramidal shape while the MWCNT coating process is carried out continuously, which leads the MWCNT framework to have the imitated shape of bipyramidal sulfur (Figure 1c). Subsequently, the sulfur particle shrinks and becomes densified, thus forming a bipyramidal S-MWCNT particle with a sulfur-free region at the edges of MWCNT framework (Figure 1d and Supporting Information, Figure S1c). The SDS and PEG are then removed during the washing and filtration process.

2.2. Characterizations of S-MWCNT and S-MWCNT with KB carbon (S-MWCNT/KB)

Figure 2a and Figure S1c (Supporting Information) show uniform morphology and size of the S-MWCNT particles performed using scanning electron microscopy (SEM). The MWCNT framework has an axial diameter (a) of 13 ± 1.0 μm and a length (l) of 20 ± 1.0 μm, which contains the identical shaped inner particle with (a) 11 ± 1.0 μm and (l) 18 ± 1.0 μm

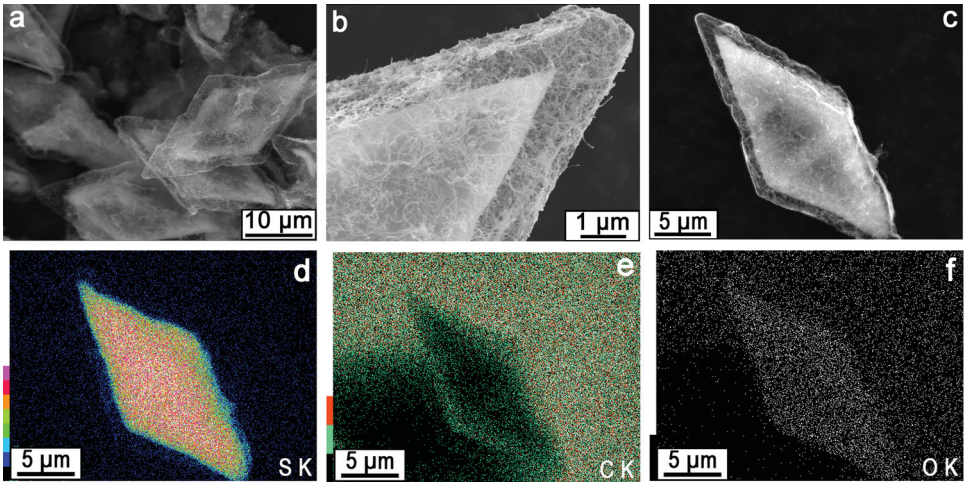

Figure 2. SEM images of S-MWCNT particles. a) Low and b) high magnification images of S-MWCNT. c) S-MWCNT on a carbon tape and corresponding element mapping images of d) sulfur, e) carbon, and f) oxygen. The color bars at the bottom left side denote the concentration of mapping elements.

(Figure 2b). Accordingly, an inner particle-free region comprising ≈35% of the volume is present along the edge of MWCNT framework. SEM images of the S-MWCNT correlated with energy dispersive X-ray spectroscopy (EDS) mapping reveal sulfur (S), carbon (C), and oxygen (O) element distribution in Figure 2c–f. The S mapping image shows the concentrated S in the inner bipyramidal particle, which is also confirmed using transmission electron microscopy (TEM) images with EDS graph (Figure S3, Supporting Information). The C concentration is relatively high at the edge of sulfur particle and sulfur-free region despite the high background intensity due to a carbon tape, while it is screened in the middle of sulfur particle. The O concentration is appreciable on the entire sulfur particle area. This O is probably acquired from oxygen functional groups on the MWCNTs formed by the acid treatment[14] but we also cannot rule out the presence of residual PEG on the sulfur despite its negligible quantity (thermogravimetric analysis (TGA), Figure S4, Supporting Information). A PEG layer on the sulfur can enclose the sulfur flexibly and alleviate the dissolution and diffusion of polysulfides.[10]

Furthermore, the 3D network structure of MWCNT framework is evidenced by a cross-sectional view of the S-MWCNT particle. The particle that was artificially cut in the middle exhibits the MWCNTs appearing from the sulfur (**Figure 3**a,b), which implies that the MWCNT networks are involved in the growth process of the sulfur. This 3D framework provides the conducting pathway in the sulfur particle as well as in the sulfur-free region, which promotes the electrical and mechanical stability for the Li–S cells.[3]

The as-prepared S-MWCNT particles contain 85 wt% sulfur (TGA in Figure S4, Supporting Information) with a *Fddd* orthorhombic structure (X-ray diffraction (XRD) pattern in Figure 3d). An additional 40 wt% KB carbon[15,16] deposited on the S-MWCNT in the absence of a binder, henceforth referred to as S-MWCNT/KB, increases the electrical conductivity and obtains a total mass of ≈50 wt% sulfur. These KB carbon coat the MWCNT framework and possibly fill the sulfur-free region. A SEM image of S-MWCNT/KB in Figure 3c shows that the KB carbon completely shield the S-MWCNT particle. The XRD pattern of S-MWCNT/KB confirms disappearance of the orthorhombic sulfur crystalline and reveals only broad graphite reflections at $2\theta \approx 25$ and 43° by the KB carbon (Figure 3d). It probably arises from more than 40 times lower KB carbon density (≤50 kg m^{-3}) than sulfur (≈2000 kg m^{-3}), which provides 32 times larger volume of KB carbon deposited on the surface of micrometer sulfur particle. This shielding layer of KB carbon is expected to perform twin functions; permitting Li^+ ion and electrolyte transport to the sulfur particle, and trapping polysulfide species.[17]

2.3. Electrochemical Performance of Li–S cells Containing S-MWCNT/KB Cathodes

2.3.1. Electrochemical Tests

The S-MWCNT/KB was then employed as a cathode in Li–S cells. We used *N*-methyl-*N*-propylpiperidinium bis(trifluoromethanesulfonyl) imide (PP13-TFSI) and dimethoxyethane (DME) in a 2 to 1 volume ratio with 1 M of $LiN(CF_3SO_2)_2$ (LiTFSI) as the electrolyte, which provided suitable Li–S cell performance by the suppression of shuttle effect and Li metal corrosion.[16] The Li–S cells using the S-MWCNT/KB cathode with 1 M of LiTFSI in PP13-TFSI/DME had an open-circuit voltage (OCV) at ≈3.0 V versus Li/Li^+ that was stably maintained. A cyclic voltammetry (CV) curve in the voltage range of 1.5–3.0 V (solid line) exhibits two cathodic (reduction) peaks at ≈2.3 and 2.0 V and typical one anodic (oxidation) peak at ≈2.4 V with a high peak-current at a sweeping rate of 0.1 mV s^{-1} (**Figure 4**a). These peaks correspond to two reduction steps ($S_8 \rightarrow Li_2S_x$ ($4 \le x \le 8$) $\rightarrow$ Li_2S_2/Li_2S) and typical one oxidation ($Li_2S_2/Li_2S \rightarrow Li_2S_x$) whereas a CV curve at slower sweeping rate reveals the additional second oxidation peak ($Li_2S_x \rightarrow S_8$) incorporated with the first oxidation peak (Figure S5, Supporting Information). Galvanostatic discharge/charge profiles in Figure 4b, recorded from 0.05 to 1 C sequentially, show two pairs of discharge/charge plateaus with respect to the Li–S redox reactions. The S-MWCNT/KB cathode in the Li–S cell delivers a discharge capacity of ≈1600 mAh g^{-1} at 0.05 C on the first cycle, which approaches ≈96% theoretical specific capacity and ≈98%

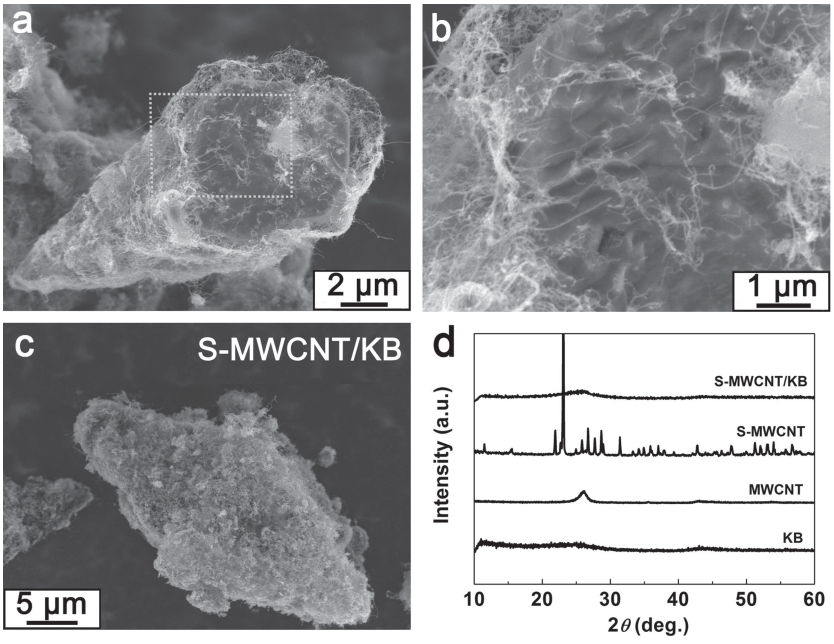

Figure 3. SEM images and XRD patterns of S-MWCNT and S-MWCNT/KB. a,b) Cross-sectional views of S-MWCNT particle that was artificially cut. b) High-magnification image of the dashed box in a). c) Top view of S-MWCNT/KB particle. d) XRD patterns of KB, MWCNT, S-MWCNT, and S-MWCNT/KB.

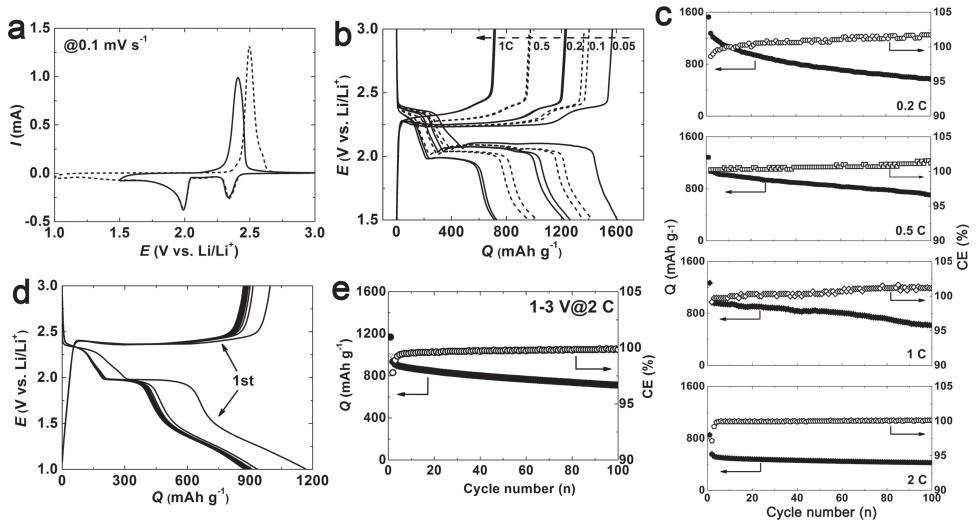

Figure 4. Li–S cell performances using S-MWCNT/KB cathodes with 1 M of LiTFSI in PP13-TFSI/DME (2/1, v/v). a) CV curves at a sweeping rate of 0.1 mV s^{-1} in 1.5–3.0 V (solid line) and 1.0–3.0 V vs Li/Li^+ (dashed line). b) Galvanostatic discharge/charge profiles sequentially recorded at current rates from 0.05 (initial cycle) to two-cycled 0.1, 0.2, 0.5, and 1 C. c) Cyclic performance and Coulombic efficiency (CE) profiles at 0.2, 0.5, 1, and 2 C (from top to bottom) during 100 cycles. d) Galvanostatic curves for 10 cycles and e) cyclic performance for 100 cycles, in 1.0–3.0 V at 2 C.

Coulombic efficiency. The cyclic performances in Figure 4c shows a discharge capacity of ≈580 mAh g^{-1} after 100 cycles at 0.2 C. The capacity retention increases at moderate current rates, resulting in 600–700 mAh g^{-1} with ≈101% Coulombic efficiency after 100 cycles at 0.5–1 C. At a high current rate of 2 C, the capacity was notably stable (≈76% retention after 100 cycles with respect to the capacity after the second cycle) and maintains ≈100% Coulombic efficiency for cycling. These cyclic performances at different current rates are not significantly altered with higher quantity of sulfur in the S-MWCNT/KB cathode. Figure S6 (Supporting Information) exhibits almost identical capacity retention but smaller rate capability from 60 wt% sulfur after 100 cycles.

This superior high rate performance is attributed to the 3D MWCNT framework, which can maintain the electrical conductivity by direct contact of the discharge products with the MWCNT network. Electrochemical impedance spectroscopy (EIS) in Figure S7 (Supporting Information) shows an Ohmic resistance of 4 Ω at the intersection with the Z' axis at high frequency, which implies an electrical conductivity of ≈0.06 S m^{-1}. The moderate MWCNT density in the framework permits great accessibility of the electrolyte and Li^+ ion with the rapid diffusion[4] while the KB carbon shield aids in alleviating the shuttle effect by trapping the polysulfides.[10] This resultant performance could not be achieved from simple physical mixing of sulfur, MWCNTs and KB carbon (S/MWCNT/KB). SEM images in Figure S8 (Supporting Information) show irregular shape and size of the S/MWCNT/KB with ≈50 wt% sulfur (≈10 μm size), 10 wt% MWCNTs and 40 wt% KB carbons. The MWCNT/KB does not shield the sulfur particle densely and some portions of sulfur particle are even exposed. Galvanostatic cell performance exhibits poor initial capacity and stability for 100 cycles. In particular, the discharge capacity at 2 C approaches almost zero after 100 cycles, which probably arises from damage to the cathode structure by the extensive shuttle effect.

2.3.2. Cycling Performance During Deep 100 Cycles

By virtue of the 3D MWCNT framework, the S-MWCNT/KB cathode enables improvement of capacity further by deep discharge in the Li–S cells. Discharge, to lower than ≈2.0 V, promotes the reduction of Li_2S_2 to Li_2S, which is a sluggish reaction due to the slow diffusion of insoluble Li_2S_2 and its low electrical conductivity.[1] This deep discharge can give rise to high overpotential during charge and poor cyclic performance due to the difficulty of Li_2S oxidation despite the increase of specific capacity. However, the 3D conducting framework enclosing both the sulfur particle and sulfur-free region is expected to afford the smooth Li–S electrochemical reaction. Figure 4a shows the CV curve (dashed line) with two cathodic peaks (2.3 and 2.0 V) and an additional broad peak in 1.75–1.25 V in a sweeping voltage range of 1.0–3.0 V. The anodic peak (2.5 V) with high peak-current shifts positively by ≈0.1 V compared to that in a sweeping voltage range of 1.5–3.0 V (solid line) and incorporates a second small oxidation peak (shoulder), which arises from the oxidation resistance of insoluble and poorly conductive Li_2S. Galvanostatic profiles in Figure 4d show a discharge curve tail below ≈1.7 V at 2 C due to the resistive discharge products.[18] Upon charge, a single plateau (≈2.36 V) is present, which is just ≈0.05 V higher than the first plateau voltage (≈2.31 V) but lower than the second plateau (≈2.43 V) performed in the voltage range 1.5–3.0 V. Consequently, both potentiostatic and galvanostatic measurements demonstrate the acceptable oxidation over-potential even in an extended potential window. Figure 4d reveals stable discharge/charge profiles with 99–100% Coulombic efficiency after the second cycle. In addition, the discharge capacity (≈870 mAh g^{-1}) is increased by a factor of around 2 compared to the one in 1.5–3.0 V (≈490 mAh g^{-1}) after 10 cycles. The cyclic performance result in Figure 4e exhibits ≈76% capacity retention after 100 cycles with respect to the capacity after the second cycles and ≈100% Coulombic efficiency. These results demonstrate great contributions of the 3D

MWCNT framework with the sulfur-free region and of the KB carbon shield with regard to the reversible Li–S redox reaction and the suppression of the shuttle effect, respectively.

3. Conclusions

In summary, we demonstrated a high performance Li–S cell with bipyramidal shaped S-MWCNT/KB containing 50–60 wt% sulfur. The 3D MWCNT framework and sulfur-free region were key to achieve stable cyclic performance with ≈100% Coulombic efficiency. In addition, the KB carbon layers shielded the active material to mitigate the shuttle effect. The specific capacity could be further improved by deep discharge/charge, which still maintained stable cycling performance with the reversible Li–S electrochemical reaction. This S-MWCNT/KB was particularly suitable for high rate performance due to the moderate density of MWCNTs, which allowed rapid Li^+ ion and electrolyte diffusion. We expect that a higher quantity of MWCNT used in the synthesis would enable the preparation of a denser 3D framework, which could enhance Li–S cell performance at moderate and slow current rate. Above all, this in situ synthesis contributes to the simple construction of a well-defined cathode structure, thus providing benefits in reducing the number of working steps needed to prepare the Li–S battery.

4. Experimental Section

Synthesis of S-MWCNT/KB: The MWCNTs (97% purity, ≈20 nm diameter (*d*)) were acid-leached with 50 mL of concentrated HNO_3 at 120 °C for 2 h and washed with deionized (DI) water (R = 18.2 MΩ) thoroughly before use. 0.2 g of acid-leached MWCNTs were dispersed in 100 mL of DI water with 1 g of SDS and 2 g of PEG (mean molecular weight ≈ 200) then 100 mL of THF solution with 0.32 M of sulfur (99% purity, sublimed) was added rapidly under vigorous stirring (1200 rpm). The mixed solution was initially a sky blue color but returned to black after several hours. After 12 h stirring, the S-MWCNT products were washed thoroughly with DI water and ethanol via vacuum filtration, put into a freezer (0 °C) overnight, then dried in a vacuum oven at 50 °C overnight. The deposition of KB carbon (ECP-600JD) on S-MWCNT particles, providing a total ≈50 (or 60) wt% sulfur in S-MWCNT/KB, was prepared by mixing of S-MWCNT with 40 (or 30) wt% KB carbon in 1/1 volume ratio of DI water/ethanol followed by stirring for 12 h, washing, and drying.

Characterizations: The morphology and element distribution information was attained from SEM (JEOL-6335) and TEM (JEOL JEM-2100F) combined with EDS. XRD patterns (with scan rate of 4° min^{-1}) were obtained using an X-ray diffractometer (RINT2000, Rigaku) with a radiation source of Cu Kα.

Preparation of Li–S Cells: The S-MWCNT/KB in cyclopentanone, mixed at 2000 rpm for 10 min using a planetary mixer/deaerator (ARE-310, Thinky), was cast on a glassy fiber (GF/C, Whatman) and dried in the vacuum oven at 50 °C for at least 12 h. A binder was not used to prepare the S-MWCNT/KB. The Li–S cell (Tomcell) was assembled with aluminum foil, the S-MWCNT/KB on the glassy fiber, one piece of Celgard 2500 and lithium metal with 280 µL of 1 M LiTFSI with PP13-TFSI/DME (v/v = 2/1) electrolyte, in an Ar-filled glove box (<1 ppm of H_2O and O_2). All components used in the assembly were dried completely in the vacuum oven at 50 °C before being transferred into the glove box. The mass of S-MWCNT/KB cathode in the Li–S cell was ≈2 mg.

Electrochemical Performance: All electrochemical measurements were performed using a VMP3 battery testing system (Biologic Claix) and the specific capacity values were calculated based on the mass of sulfur in the cathode. All voltage values were referenced to Li/Li^+. EIS measurements were performed in the frequency range of 100 mHz–1 MHz at potentiostatic signal amplitudes of 5 mV.

Supporting Information

Supporting Information is available from the Wiley Online Library or from the author.

Acknowledgements

This work was financially supported by RIKEN and Fund for Seeds of Collaborative Research.

Received: August 20, 2013
Revised: October 21, 2013
Published online: December 2, 2013

[1] X. Ji, L. F. Nazar, *J. Mater. Chem.* **2010**, *20*, 9821.
[2] P. G. Bruce, S. A. Freunberger, L. J. Hardwick, J.-M. Tarascon, *Nat. Mater.* **2011**, *11*, 19.
[3] X. Ji, K. T. Lee, L. F. Nazar, *Nat. Mater.* **2009**, *8*, 500.
[4] G. He, X. Ji, L. F. Nazar, *Energy Environ. Sci.* **2011**, *4*, 2878.
[5] a) R. Demir-Cakzn, M. Morcrette, F. Nouar, C. Davoisne, T. Devic, D. Gonbeau, R. Dominko, C. Serre, G. Ferey, J.-M. Tarascon, *J. Am. Chem. Soc.* **2011**, *133*, 16154; b) K. Xi, S. Cao, X. Peng, C. Ducati, R. V. Kumar, A. K. Cheetham, *Chem. Commun.* **2013**, *49*, 2192.
[6] G. Zheng, Y. Yang, J. J. Cha, S. S. Hong, Y. Cui, *Nano Lett.* **2011**, *11*, 4462.
[7] a) R. Elazari, G. Salitra, A. Garsuch, A. Panchenko, D. Aurbach, *Adv. Mater.* **2011**, *23*, 5641; b) L. Ji, M. Rao, S. Aloni, L. Wang, E. J. Cairnsb, Y. Zhang, *Energy Environ. Sci.* **2011**, *4*, 5053.
[8] a) L. Xiao, Y. Cao, J. Xiao, B. Schwenzer, M. H. Englhard, L. V. Saraf, Z. Nie, G. J. Exarhos, J. Liu, *Adv. Mater.* **2012**, *24*, 1176; b) Y. Fu, A. Manthiram, *J. Phys. Chem. C* **2012**, *116*, 8910; c) J. Guo, Z. Yang, Y. Yu, H. D. Abruña, L. A. Archer, *J. Am. Chem. Soc.* **2013**, *135*, 763.
[9] W. Li, G. Zheng, Y. Yang, Z. W. Seh, L. Nian, Y. Cui, *Proc. Natl. Acad. Sci.* **2013**, *110*, 7148.
[10] H. Wang, Y. Yang, Y. Liang, J. T. Robinson, Y. Li, A. Jackson, Y. Cui, H. Dai, *Nano Lett.* **2011**, *11*, 2644.
[11] a) L. Ji, M. Rao, H. Zheng, L. Zhang, Y. Li, W. Duan, J. Guo, E. J. Cairns, Y. Zhang, *J. Am. Chem. Soc.* **2011**, *133*, 18522; b) Y. Cao, X. Li, I. A. Aksay, J. Lemmon, Z. Nie, Z. Yang, J. Liu, *Phys. Chem. Chem. Phys.* **2011**, *13*, 7660; c) L. Zhang, L. Ji, P.-A. Glans, Y. Zhang, J. Zhu, J. Guo, *Phys. Chem. Chem. Phys.* **2012**, *14*, 13670.
[12] S. Evers, L. F. Nazar, *Chem. Commun.* **2012**, *48*, 1233.
[13] W. Wei, V. G. Pol, K. Amine, *Adv. Mater.* **2013**, *25*, 1608.
[14] G. Trykowski, S. Biniak, L. Stobinski, B. Lesiak, *Acta Phys. Pol. A* **2010**, *118*, 515.
[15] a) R. Demir-Cakzn, M. Morcrette, Gangulibabu, A. Guéguen, R. Dedryvère, J.-M. Tarascon, *Energy Environ. Sci.* **2013**, *6*, 176; b) J. Zheng, M. Gu, M. J. Wagner, K. A. Hays, X. Li, P. Zuo, C. Wang, J.-G. Zhang, J. Liu, J. Xiao, *J. Electrochem. Soc.* **2013**, *160*, A1624.
[16] L. Wang, H. R. Byon, *J. Power Sources* **2013**, *236*, 207.
[17] J. Nelson, S. Misra, Y. Yang, A. Jackson, Y. Liu, H. Wang, H. Dai, J. C. Andrews, Y. Cui, M. F. Toney, *J. Am. Chem. Soc.* **2012**, *134*, 6337.
[18] J. Kim, D.-J. Lee, H.-G. Jung, Y.-K. Sun, J. Hassoun, B. Scrosati, *Adv. Funct. Mater.* **2013**, *23*, 1076.